Solutions of conformal Israel-Stewart relativistic viscous fluid dynamics

Hugo Marrochio,[1] Jorge Noronha,[1] Gabriel S. Denicol,[2] Matthew Luzum,[2,3] Sangyong Jeon,[2] and Charles Gale[2]
[1]*Instituto de Física, Universidade de São Paulo, C.P. 66318, 05315-970 São Paulo, São Paulo, Brazil*
[2]*Department of Physics, McGill University, 3600 University Street, Montreal, Quebec H3A 2T8, Canada*
[3]*Lawrence Berkeley National Laboratory, Nuclear Science Division, MS 70R0319, Berkeley, California 94720, USA*
(Received 7 August 2013; revised manuscript received 9 December 2014; published 16 January 2015)

We use symmetry arguments developed by Gubser to construct the first radially expanding explicit solutions of the Israel-Stewart formulation of hydrodynamics. Along with a general semi-analytical solution, an exact analytical solution is given which is valid in the cold plasma limit where viscous effects from shear viscosity and the relaxation time coefficient are important. The radially expanding solutions presented in this paper can be used as nontrivial checks of numerical algorithms employed in hydrodynamic simulations of the quark-gluon plasma formed in ultrarelativistic heavy ion collisions. We show this explicitly by comparing such analytic and semi-analytic solutions with the corresponding numerical solutions obtained using the MUSIC viscous hydrodynamics simulation code.

DOI: 10.1103/PhysRevC.91.014903 PACS number(s): 12.38.Mh, 47.75.+f, 47.10.ad, 11.25.Hf

I. INTRODUCTION

Our current understanding of the novel properties displayed by the quark-gluon plasma (QGP) formed in ultrarelativistic heavy ion collisions [1] relies heavily on solving relativistic dissipative fluid dynamics [2,3]. The equations of relativistic fluid dynamics form a set of complicated nonlinear partial differential equations, describing the conservation of energy-momentum and a conserved charge (such as net baryon number),

$$\partial_\mu T^{\mu\nu} = 0, \quad \partial_\mu N^\mu = 0.$$

In the presence of dissipation, the above equations are not closed and have to be supplemented by nine additional equations of motion, i.e., the time evolution equations for the the bulk viscous pressure, heat flow, and shear-stress tensor.

The simplest formulation of relativistic dissipative fluid dynamics are the Navier-Stokes equations. However, due to instabilities and acausal signal propagation in these equations [4], they are not usually used in numerical simulations. Currently, most fluid-dynamical simulations of the QGP employ the relaxation-type equations derived by Israel and Stewart [5] to close the conservation laws. While some analytic solutions of the non-relativistic Navier-Stokes equations are widely known [6], very few analytical (or semi-analytical) solutions of relativistic fluid dynamics [7–10] have been obtained and most simulations of heavy ion collisions solve dissipative fluid dynamics numerically. Clearly, it would be useful to have solutions of Israel-Stewart theory in any limit, especially in the cases relevant to heavy ion collision applications.

In Refs. [11,12], Gubser and Yarom derived $SO(3) \otimes SO(1,1) \otimes Z_2$ invariant solutions of ideal relativistic conformal fluid dynamics and relativistic Navier-Stokes theory. In this paper we use the same symmetry arguments to derive solutions of Israel-Stewart theory, which can be relevant to the description of a conformal QGP. Like the well known Bjorken solution [7], the fluid dynamic variables in the dissipative solutions we obtain are invariant under Lorentz boosts in one direction, which is a symmetry that seems to be (approximately) satisfied in heavy ion collisions near mid-rapidity. However, unlike the Bjorken solution, the solutions discussed here also have nontrivial (transverse) radial expansion.

Thus, the solutions found in this paper provide the most rigorous tests to date for the current numerical algorithms used to solve the viscous relativistic fluid dynamic equations in heavy ion collisions. We show this explicitly by comparing multi-dimensional numerical solutions obtained using MUSIC, a 3+1-dimensional (3+1D) viscous hydrodynamics simulation code [13], with the analytical and semi-analytical solutions of Israel-Stewart-like theories undergoing Gubser flow. We remark that the version of MUSIC employed in this work is an updated version currently being maintained at McGill University.

This paper is organized as follows. In the next section we briefly introduce the equations of relativistic dissipative fluid dynamics and describe the solution for the flow velocity obtained by Gubser. In Sec. III we derive the main results of this paper and solve the equations of motion of Israel-Stewart theory undergoing Gubser flow. We show in Sec. IV how these solutions can be used to test numerical simulations of relativistic fluid dynamics. We conclude with a summary of our results.

II. HYDRODYNAMICS FOR HEAVY ION COLLISIONS AND GUBSER FLOW

In ultra-relativistic heavy ion applications, relativistic fluid dynamics is more naturally described in hyperbolic coordinates $x^\mu = (\tau, r, \phi, \xi)$ where the line element is $ds^2 = -d\tau^2 + dr^2 + r^2 d\phi^2 + \tau^2 d\xi^2$, $r = \sqrt{x^2 + y^2}$, and ϕ parametrize the transverse plane perpendicular to the beam direction, while $\tau = \sqrt{t^2 - z^2}$ and the rapidity $\xi = 1/2 \times \ln[(t+z)/(t-z)]$ are given in terms of usual coordinates t and the beam direction z.

The minimum set of relaxation-type equations for a viscous conformal fluid is [14]

$$\frac{D_\tau T}{T} + \frac{1}{3}\nabla_\alpha u^\alpha + \frac{\pi_{\mu\nu}\sigma^{\mu\nu}}{3sT} = 0\,, \tag{1}$$

$$\frac{\Delta^\mu_\alpha \nabla^\alpha T}{T} + D_\tau u^\mu + \frac{\Delta^\mu_\nu \nabla_\alpha \pi^{\alpha\nu}}{sT} = 0\,, \tag{2}$$

$$\frac{\tau_R}{sT}\left(\Delta^\mu_\alpha \Delta^\nu_\beta\, D_\tau \pi^{\alpha\beta} + \frac{4}{3}\pi^{\mu\nu}\nabla_\alpha u^\alpha\right) + \frac{\pi^{\mu\nu}}{sT} = -\frac{2\eta}{s}\frac{\sigma^{\mu\nu}}{T}, \tag{3}$$

where ∇_μ is the space-time covariant derivative, T is the local temperature, u^μ is the four-velocity of the fluid ($u_\mu u^\mu = -1$), and $\pi^{\mu\nu}$ is the shear-stress tensor. We use natural units $\hbar = c = k_B = 1$. The metric tensor in flat space-time is $g_{\mu\nu} = \mathrm{diag}\,(-,+,+,+)$. We further introduced the entropy density $s \sim T^3$, the shear viscosity coefficient η, the shear relaxation time τ_R, the spatial projector $\Delta_{\mu\nu} \equiv g_{\mu\nu} + u_\mu u_\nu$, the comoving derivative $D_\tau \equiv u^\lambda \nabla_\lambda$, and the shear tensor $\sigma^{\mu\nu} \equiv \Delta^{\mu\nu\alpha\beta}\nabla_\alpha u_\beta$, with $\Delta^{\mu\nu\alpha\beta} \equiv (\Delta^{\mu\alpha}\Delta^{\nu\beta} + \Delta^{\mu\beta}\Delta^{\nu\alpha})/2 - \Delta^{\mu\nu}\Delta^{\alpha\beta}/3$ being the double, symmetric, traceless projection operator. Even though other terms can be included in the dynamical equation for the shear-stress tensor [14,15], for simplicity in this paper we consider only the terms present in (3).

Equation (3) contains two transport coefficients, η and τ_R. In a conformal fluid, the shear viscosity coefficient is always proportional to the entropy density, $\eta \sim s$, while the shear relaxation time must be proportional to the inverse of the temperature, $\tau_R \sim 1/T$. Without loss of generality, the relaxation time is parametrized as

$$\tau_R = c\,\frac{\eta}{Ts}, \tag{4}$$

where c is a constant.

We shall consider here the case in which the dynamics is boost invariant and the flow is radially symmetric, i.e., $T = T(\tau,r)$ and $\pi^{\mu\nu} = \pi^{\mu\nu}(\tau,r)$. These conditions are approximately met near mid-rapidity in ultracentral collisions at the Large Hadron Collider (LHC), recently measured by the ATLAS and CMS Collaborations [16,17]. In order to obtain analytical solutions, we will follow [11] and further assume that the conformal fluid flow is actually invariant under $\mathrm{SO}(3) \otimes \mathrm{SO}(1,1) \otimes \mathrm{Z}_2$. The SO(3) piece is a subgroup of the SO(4,2) conformal group which describes the symmetry of the solution under rotations around the beam axis and two operations constructed using special conformal transformations that replace translation invariance in the transverse plane. For more details regarding the generators of the SO(3) symmetry group of this solution, see Ref. [11]. The Z_2 piece stands for invariance under $\xi \to -\xi$, while SO(1,1) denotes invariance under boosts along the beam axis. In this case, the dynamical variables depend on τ and r through the dimensionless combination [11,12]

$$\rho = \sinh^{-1}\left(-\frac{1-\tilde\tau^2+\tilde r^2}{2\tilde\tau}\right), \tag{5}$$

where $\tilde\tau \equiv q\tau$ and $\tilde r = qr$, with q being an arbitrary inverse-length scale. Without loss of generality, we set $q = 1\,\mathrm{fm}^{-1}$ when solving the fluid-dynamical equations. Furthermore, the flow is completely determined by symmetry constraints to be [11,12]

$$\begin{aligned} u_\tau &= -\cosh\left[\tanh^{-1}\left(\frac{2\tilde\tau\tilde r}{1+\tilde\tau^2+\tilde r^2}\right)\right], \\ u_r &= \sinh\left[\tanh^{-1}\left(\frac{2\tilde\tau\tilde r}{1+\tilde\tau^2+\tilde r^2}\right)\right], \\ u_\phi &= u_\xi = 0\,. \end{aligned} \tag{6}$$

In the following, this solution will be referred to as Gubser flow. Since the flow is known, the relativistic Euler equation (2) is automatically satisfied and, thus, only the equations for the temperature (1) and the shear-stress tensor (3) need to be solved.

In order to solve the remaining equations, it is convenient to go to a different coordinate system in which the flow velocity is zero. For this purpose, one must first perform a Weyl rescaling of the metric, $ds^2 \to d\hat s^2 \equiv ds^2/\tau^2$, which is the metric in $\mathrm{dS}_3 \otimes \mathbf{R}$, with dS_3 corresponding to the three-dimensional de Sitter space. Then one can implement the coordinate transformation introduced in [12],

$$\sinh\rho = -\frac{1-\tilde\tau^2+\tilde r^2}{2\tilde\tau}\,, \quad \tan\theta = \frac{2\tilde r}{1+\tilde\tau^2-\tilde r^2}\,, \tag{7}$$

which takes $d\hat s^2$ to $d\hat s^2 = -d\rho^2 + \cosh^2\rho\, d\theta^2 + \cosh^2\rho\sin^2\theta\, d\phi^2 + d\xi^2$. In this coordinate system the fluid is at rest and, consequently, the equations of motion for ε and $\pi^{\mu\nu}$ considerably simplify, making it possible to find analytical and semi-analytical solutions of Israel-Stewart theory.

In the following, we denote all fluid-dynamical variables in this new coordinate system with a hat (circumflex). As mentioned, such generalized de Sitter coordinate is extremely convenient since it leads to a static velocity profile, i.e., $\hat u_\mu = (-1,0,0,0)$, and considerably simplifies the calculations. As already mentioned, the fields are only functions of ρ, i.e, $\hat T = \hat T(\rho)$ and $\hat\pi^{\mu\nu} = \hat\pi^{\mu\nu}(\rho)$. Because of the metric rescaling and the coordinate transformation $x^\mu = (\tau,r,\phi,\xi) \to \hat x^\mu(\rho,\theta,\phi,\xi)$, the dimensionless dynamical variables in $\mathrm{dS}_3 \otimes \mathbf{R}$ are related to those in hyperbolic coordinates as follows:

$$u_\mu(\tau,r) = \tau\frac{\partial \hat x^\nu}{\partial x^\mu}\hat u_\nu\,, \tag{8}$$

$$T(\tau,r) = \frac{\hat T}{\tau}\,, \tag{9}$$

$$\pi_{\mu\nu}(\tau,r) = \frac{1}{\tau^2}\frac{\partial \hat x^\alpha}{\partial x^\mu}\frac{\partial \hat x^\beta}{\partial x^\nu}\hat\pi_{\alpha\beta}\,. \tag{10}$$

The factors of τ in the transformation rules above come from the known properties of these fields under Weyl transformations [12]. For instance, since $\pi_{\mu\nu} \to \Omega^2\pi_{\mu\nu}$ under Weyl rescaling $g_{\mu\nu} \to \Omega^{-2} g_{\mu\nu}$ with $\Omega = \tau$, there is a factor of $1/\tau^2$ in (10). Given the dictionary between the fields in the different spaces shown above, one can solve the Eqs. (1) and (3) in $\mathrm{dS}_3 \otimes \mathbf{R}$ where the fluid is static and the fields are homogeneous (i.e., they only depend on the de Sitter time coordinate ρ) and plug in the solutions to find the fields in the standard flat space-time. This is the general strategy that we

shall follow below to find solutions for the viscous relativistic fluid defined above.

We emphasize that the Gubser flow solution described so far does assume symmetries that are not strictly present in realistic ultracentral heavy ion collisions, such as conformal symmetry. Despite this fact, it can still be useful to understand the solutions of relativistic fluid dynamics on a qualitative level and also, as will be shown in this paper, to test numerical simulations of relativistic fluid dynamics in a setting similar to that created in a heavy ion collision.

III. ISRAEL-STEWART THEORY

In this section we derive for the first time the solutions of Israel-Stewart theory in the Gubser flow regime. These solutions shall be later compared to numerical simulations of fluid dynamics. It is straightforward to work out the equations of motion for $\hat{T}(\rho)$ and $\hat{\pi}^{\mu}_{\nu}(\rho)$ in the generalized de Sitter coordinates. First, note that orthogonality to the flow gives $\hat{\pi}^{\mu}_{\rho}=0$ (where $\mu=\rho,\theta,\phi,\xi$) while the tracelessness condition imposes $\hat{\pi}^{\xi}_{\xi}=-\hat{\pi}^{\theta}_{\theta}-\hat{\pi}^{\phi}_{\phi}$. Since the only nonzero components of the shear tensor are $\hat{\sigma}^{\xi}_{\xi}=-2\tanh\rho/3, \hat{\sigma}^{\theta}_{\theta}=\hat{\sigma}^{\phi}_{\phi}=\tanh\rho/3$, each one of the of-diagonal terms of the $\hat{\pi}^{\mu}_{\nu}$ tensor follows an independent, first-order linear homogeneous equation and we set their initial conditions to zero (thus, they do not contribute to the dynamics). One can show that $\hat{\pi}^{\theta}_{\theta}$ and $\hat{\pi}^{\phi}_{\phi}$ obey the same differential equations and, since we impose the same initial conditions for these fields, $\hat{\pi}^{\xi}_{\xi}=-2\hat{\pi}^{\theta}_{\theta}=-2\hat{\pi}^{\phi}_{\phi}$. We then find that the only nontrivial nonlinear equations of motion are

$$\frac{1}{\hat{T}}\frac{d\hat{T}}{d\rho}+\frac{2}{3}\tanh\rho=\frac{1}{3}\bar{\pi}^{\xi}_{\xi}(\rho)\tanh\rho\,, \quad (11)$$

$$\frac{c}{\hat{T}}\frac{\eta}{s}\left[\frac{d\bar{\pi}^{\xi}_{\xi}}{d\rho}+\frac{4}{3}\left(\bar{\pi}^{\xi}_{\xi}\right)^2\tanh\rho\right]+\bar{\pi}^{\xi}_{\xi}=\frac{4}{3}\frac{\eta}{s\hat{T}}\tanh\rho\,, \quad (12)$$

where $\bar{\pi}^{\xi}_{\xi}\equiv\hat{\pi}^{\xi}_{\xi}/(\hat{T}\hat{s})$. This variable is convenient since it is invariant under Weyl transformations. In order to derive the equations above we used that $\hat{\nabla}_{\alpha}\hat{u}^{\alpha}=2\tanh\rho$.

Note that for any nonzero τ, the value of ρ decreases with r, while for a fixed r the value of ρ increases with τ. Thus, when $\rho\ll 0$ one probes regions in which $r\gg 1$, and when $\rho\gg 1$ one has $\tau\gg 1$. In this sense, we expect that physically meaningful solutions behave as $\lim_{\rho\to\pm\infty}\hat{T}(\rho)=0$, i.e., at an infinite radius or time the temperature should go to zero. On the other hand, given the definition of $\bar{\pi}^{\xi}_{\xi}$, it is consistent to have $\lim_{\rho\to\pm\infty}\bar{\pi}^{\xi}_{\xi}(\rho)$ finite and nonzero ($\bar{\pi}^{\xi}_{\xi}$ is a ratio between two quantities that should vanish when $\rho\to\pm\infty$).

In the ideal fluid limit $\bar{\pi}^{\xi}_{\xi}=0$ and we have only a single equation left over for the temperature. The analytical solution is the one found in [11,12],

$$\hat{T}_{\rm ideal}(\rho)=\frac{\hat{T}_0}{\cosh^{2/3}\rho}\,, \quad (13)$$

where $\hat{T}_0\equiv\hat{T}_{\rm ideal}(0)$ is a positive constant (so then $\hat{T}_{\rm ideal}$ is positive-definite). Using the dictionary in (9), we see that the temperature in the original hyperbolic coordinates is given by

$$T_{\rm ideal}(\tau,r)=\frac{\hat{T}_0(2q\tau)^{2/3}}{\tau[1+2q^2(\tau^2+r^2)+q^4(\tau^2-r^2)^2]^{1/3}}, \quad (14)$$

and, at the time $\tau_0=1/q$, one finds $T_{\rm ideal}(\tau_0,0)=\hat{T}_0\,q$.

The relativistic Navier-Stokes approximation to our set of equations consists in setting the relaxation time to zero, i.e., $\tau_R=0$, while keeping η/s nonzero in (12). In this case, $\bar{\pi}^{\xi}_{\xi}(\rho)=4/(3\hat{T})\times(\eta/s)\tanh\rho$ and the equation of motion for $\hat{T}$ becomes

$$\frac{d}{d\rho}\hat{T}+\frac{2}{3}\hat{T}\tanh\rho=\frac{4}{9}\frac{\eta}{s}(\tanh\rho)^2.$$

The analytical solution, previously found in [11,12], is

$$\hat{T}_{\rm NS}(\rho)=\frac{\hat{T}_0}{\cosh^{2/3}\rho}+\frac{4}{27}\frac{\eta}{s}\frac{\sinh^3\rho}{\cosh^{2/3}\rho}\times{}_2F_1\left(\frac{3}{2};\frac{7}{6};\frac{5}{2};-\sinh^2\rho\right), \quad (15)$$

where ${}_2F_1$ is a hypergeometric function. From the equation of motion, the condition $\lim_{\rho\to\pm\infty}\hat{T}'_{\rm NS}(\rho)=0$ shows that $\lim_{\rho\to\pm\infty}\hat{T}_{\rm NS}(\rho)=\pm 2\eta/3s$ [11,12]. In this case, once $\eta/s\neq 0$, for any given τ there is always a value of r beyond which the temperature switches sign and becomes negative (which is very different than the ideal case in which $\lim_{\rho\to\pm\infty}\hat{T}_{\rm ideal}=0$). This effect may be connected with the well known causality issue (see, for instance, [18,19]) of the relativistic Navier-Stokes equations. We shall see below that once the relaxation time coefficient is taken into account one can find a solution where $\hat{T}$ is positive-definite and $\lim_{\rho\to-\infty}\hat{T}(\rho)=0$.

Obtaining solutions of Israel-Stewart theory is more evolved, since the relaxation time in Eq. (12) cannot be set to zero, i.e., $\tau_R\neq 0$. In this case $\bar{\pi}^{\xi}_{\xi}$ obeys a differential equation (which requires an independent initial condition) and the set of equations becomes nonlinear. At the very least, it is possible to find one qualitative difference between the asymptotic solutions ($\lim_{\rho\to\pm\infty}$) of Navier-Stokes and Israel-Stewart theories. If one imposes that $\lim_{\rho\to\pm\infty}\hat{T}(\rho)=0$ and, simultaneously, $\lim_{\rho\to\pm\infty}d\bar{\pi}^{\xi}_{\xi}(\rho)/d\rho=0$, one can find the asymptotic solution for $\bar{\pi}^{\xi}_{\xi}(\rho)$, $\lim_{\rho\to\pm\infty}|\bar{\pi}^{\xi}_{\xi}(\rho)|=\sqrt{1/c}$ [note that the parameter c appeared in the definition of the relaxation time; see Eq. (4)]. Therefore, in contrast to Navier-Stokes theory, solutions in which $\lim_{\rho\to\pm\infty}\hat{T}(\rho)=0$ are possible in Israel-Stewart theory and do happen in practice as long as τ_R is nonzero.

There is a limit in which one can find analytical solutions for $\hat{T}$ and $\bar{\pi}^{\xi}_{\xi}$. This becomes possible when the fluid is very viscous or when the temperature is very small, i.e., when $\eta/(s\hat{T})\gg 1$. In this case, called here the *cold plasma limit*, the term $\bar{\pi}^{\xi}_{\xi}$ becomes negligible in comparison to all the other terms in Eq. (12), which are all linear in $\eta/(s\hat{T})$. In this limit, one can directly solve the equation for $\bar{\pi}^{\xi}_{\xi}$ to find

$$\bar{\pi}^{\xi}_{\xi}(\rho)=\sqrt{\frac{1}{c}}\tanh\left[\sqrt{\frac{1}{c}}\left(\frac{4}{3}\ln\cosh\rho-\bar{\pi}_0 c\right)\right], \quad (16)$$

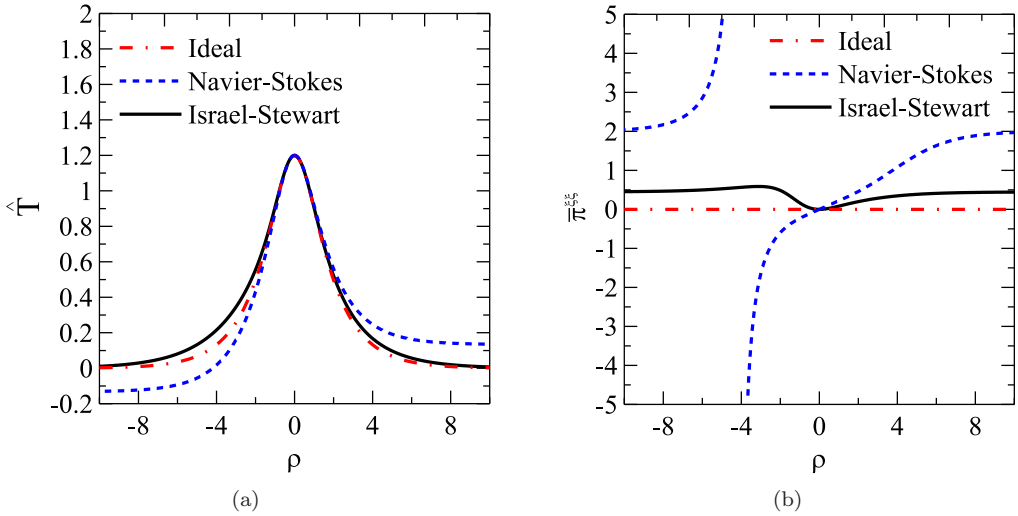

FIG. 1. (Color online) Comparison between the solutions for $\hat{T}$ (left panel) and $\bar{\pi}^{\xi}_{\xi}$ (right panel) for $\eta/s = 0.2, c = 5$, and $\hat{T}(0) = 1.2$ found using different versions of the relativistic fluid equations. The solid black lines denote solutions of Israel-Stewart theory, results from relativistic Navier-Stokes theory are in dashed blue, while the dashed-dotted red curves correspond to the ideal fluid case.

where $\bar{\pi}_0$ is a constant and, substituting this into Eq. (11), we obtain

$$\hat{T}(\rho) = \hat{T}_1 \frac{\exp(c\bar{\pi}_0/2)}{(\cosh\rho)^{2/3}} \cosh^{1/4}\left[\sqrt{\frac{1}{c}}\left(\frac{4}{3}\ \ln\cosh\rho - \bar{\pi}_0 c\right)\right]. \tag{17}$$

where $\hat{T}_1$ is a constant. These analytical solutions are even in $\rho, \hat{T}$ is positive-definite, and $\lim_{\rho\to\pm\infty}\hat{T}(\rho) = 0$ if $4c > 1$. Moreover, note that as long as $c > 1, \bar{\pi}^{\xi}_{\xi}$ is always smaller than 1 for any value of ρ, i.e, the dissipative correction to the energy-momentum tensor is always smaller than the ideal fluid contribution. In the next section, the analytical solutions in Eqs. (16) and (17) will be compared to numerical solutions of fluid dynamics obtained with MUSIC.

We show in Fig. 1 a comparison between $\hat{T}$ and $\bar{\pi}^{\xi}_{\xi}$ computed for an ideal fluid, Navier-Stokes theory, and Israel-Stewart theory for $\eta/s = 0.2$, which is a value in the ballpark of that normally used in hydrodynamic simulations of the QGP in heavy ion collisions [20], and $c = 5$, which is the typical value obtained from approximations of the Boltzmann equation [21–23]. The equation of state employed is that of an ideal gas of massless quarks and gluons,

$$\varepsilon = 3\left[2\left(N_C^2 - 1\right) + \frac{7}{2}N_C N_F\right]\frac{\pi^2}{90}T^4,$$

where $N_C = 3$ and $N_F = 2.5$. We have chosen the initial conditions for the equations such that $\hat{T}(0) = 1.2$, for all the cases, and, for the Israel-Stewart case, $\bar{\pi}^{\xi}_{\xi}(0) = 0$. We solve Eqs. (11) and (12) numerically using MATHEMATICA's NDSolve subroutine. The Israel-Stewart theory results are shown in solid black, the Navier-Stokes results in dashed blue, and the ideal fluid result in the dashed-dotted red curve. One can see that the Israel-Stewart solution for $\hat{T}$ is positive-definite and $\lim_{\rho\to\pm\infty}\hat{T}(\rho) = 0$. Moreover, viscous effects break the parity of the solutions with respect to $\rho \to -\rho$. Note that, as mentioned before, $\bar{\pi}^{\xi}_{\xi}$ goes to $\sqrt{1/c}$ when $\rho \to \pm\infty$ in Israel-Stewart theory while for the Navier-Stokes solution this quantity diverges at $\rho \approx -4.19$, which is the value of ρ at which $\hat{T}_{\rm NS} = 0$. We also checked that the analytical limit in Eqs. (16) and (17) matches the numerical solution for $\eta/s = 1/(4\pi)$ [24] and $c = 5$ when $\hat{T}(0) \leqslant 0.001$, i.e., when the temperature is extremely small.

In order to study the space-time dependence of the Israel-Stewart solutions we define $q = 1\,\text{fm}^{-1}$ so that $\rho = 0$ corresponds to $\tau = 1$ fm and $r = 0$. Therefore, in standard hyperbolic coordinates, $T(r = 0, \tau_0 = 1\ \text{fm}) = 1.2\,\text{fm}^{-1}$ and $\bar{\pi}^{\xi}_{\xi}(r = 0, \tau_0 = 1\ \text{fm}) = 0$. In Fig. 2 we show a comparison between the temperature profiles for Israel-Stewart theory at the times $\tau = 1.2, 1.5, 2$ fm, with $\eta/s = 0.2, c = 5$. Also, in the same figure we show $\tau^2\pi^{\xi\xi}$ as a function of the radius for the same times. The other components of the shear-stress tensor can be obtained using the dictionary in Eq. (10).

Note that the system is expanding in the transverse plane. It appears to be imploding because of the energy flowing out in the longitudinal direction. A larger viscosity might change this effect quantitatively, but the qualitatively features will remain the same.

A. Entropy production in Israel-Stewart theory under Gubser flow

It is useful to discuss the entropy production in Israel-Stewart theory when the conformal fluid described is in the Gubser flow regime. First of all, it is important to note that in Israel-Stewart theory the thermodynamic entropy, obtained from the equation of state, i.e., $s(T) = (\varepsilon + P)/T$, does not satisfy the second law of thermodynamics. As a matter of fact, Israel-Stewart theory is (phenomenologically) derived by generalizing the thermodynamic entropy so that the second law of thermodynamics is satisfied and, simultaneously, fluid-dynamical equations of motion that are causal and stable are obtained. In this approach, the entropy density and current can only be obtained approximately, up to a certain order in powers

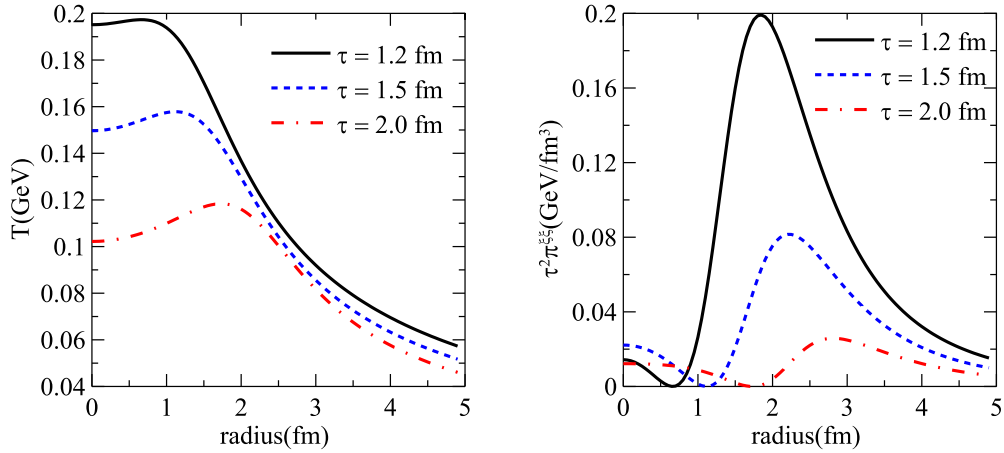

FIG. 2. (Color online) Temperature and $\tau^2\pi^{\xi\xi}$ profiles in Israel-Stewart theory for $\tau = 1.2$ fm (solid black curves), $\tau = 1.5$ fm (dashed blue curves), and $\tau = 2$ fm (dashed-dotted red curves) with $q = 1\,\text{fm}^{-1}, \eta/s = 0.2, c = 5$, and $\hat{T}(0) = 1.2$.

of the shear-stress tensor (and other dissipative currents, if they are present). Up to second order in $\pi^{\mu\nu}$, the generalized entropy current reads [5]

$$S^\mu = su^\mu - \frac{\tau_\pi}{4\eta T} u^\mu \pi_{\alpha\beta}\pi^{\alpha\beta} + \mathcal{O}(3)\,, \tag{18}$$

where $\mathcal{O}(3)$ denotes terms of third order in the dissipative currents. The nonequilibrium entropy density is obtained from S^μ as usual:

$$s_{\text{neq}} = -u_\mu S^\mu = s - \frac{\tau_\pi}{4\eta T}\pi_{\alpha\beta}\pi^{\alpha\beta} + \mathcal{O}(3)\,. \tag{19}$$

Note that here we did not consider contributions that arise from bulk viscous pressure and heat flow. The complete expansion can be found in, e.g., Ref. [5]. Also, a complete expression for the entropy current up to third order in gradients was derived in Ref. [25]. Note that, in contrast to Navier-Stokes theory, the entropy production in Israel-Stewart theory is not linearly proportional to the shear viscosity coefficient.

Using the fluid-dynamical equations described in the previous sections, Eqs. (1), (2), and (3), one can show that, up to fourth order in powers of the shear-stress tensor, the entropy production is a positive-definite quadratic function of the dissipative currents,

$$\begin{aligned}\partial_\mu S^\mu &= \frac{1}{2\eta T}\pi_{\mu\nu}\pi^{\mu\nu} - \frac{25}{12T(\varepsilon + P)^2}\pi_{\alpha\beta}\pi^{\alpha\beta}\pi_{\mu\nu}\sigma^{\mu\nu} \\ &= \frac{1}{2\eta T}\pi_{\mu\nu}\pi^{\mu\nu} + \mathcal{O}(4).\end{aligned} \tag{20}$$

Obviously this is only true since the temperature and shear viscosity are positive-definite quantities (as already discussed, negative temperatures do not appear in solutions of Israel-Stewart theory). When Israel-Stewart theory breaks down, the $\mathcal{O}(4)$ term in the equation above is not necessarily negligible and the entropy production is no longer guaranteed to be positive. We will see later that this can happen in the Israel-Stewart theory solutions presented in this paper when the value of ρ becomes very negative, i.e., at early times and/or large radius. In these regions, one should not trust the fluid-dynamical solutions, even though they can still be used for other purposes, such as testing codes.

In Fig. 3(a) we plot the generalized entropy current multiplied by $\tau r u^\tau$ as a function of the radius, r. We multiply the entropy density by the relevant phase space factors $r \times \tau$ and by the gamma factor u^τ (the factor τ is taken out from the integration in the longitudinal direction, which should be made in $\tau\xi$ and not just ξ). Due to the symmetries assumed when deriving the Gubser flow solution, s and u^τ are constant in ϕ and ξ and, hence, the integration in these variables is trivial. Thus, the total entropy is proportional to the area under the curves in Fig. 3(a).

In Fig. 3(b), we further show the entropy production, $Q = \pi_{\mu\nu}\pi^{\mu\nu}/(2\eta T)$, as a function of the radius, for several time steps. One can see that the entropy production in Gubser flow solutions is not very large, even though the system is far away from the Navier-Stokes regime. In Fig. 3(c), we show the total entropy production of the theory $Q_{\text{total}} = \pi_{\mu\nu}\pi^{\mu\nu}/(2\eta T) - 25\pi_{\alpha\beta}\pi^{\alpha\beta}\pi_{\mu\nu}\sigma^{\mu\nu}/[12T(\varepsilon + P)^2]$, which does not neglect the term of order 4, as is usually done in Israel-Stewart theory. We see that the order-4 term is not necessarily small and does affect the entropy production significantly. At late times and small values of radius, it appears as just a correction. However, at early times and large radius, the $\mathcal{O}(4)$ term is large and can even drive the entropy production term to negative values. For example, when $\tau = 1$ fm, the entropy production becomes negative when $r \gtrsim 3.5$. On the other hand, at $\tau = 2$ fm, the entropy production is always positive between $r = 0$ and 5 fm. We note that, at any time, there will always be a value of the radius for which the entropy production becomes negative. The larger the time, the larger this value of radius will be.

Note that, even though 1 fm of time evolution might appear to be small, in Gubser flow solutions it is enough time for the energy density in the center of the system to decrease by a factor 16 (and for the temperature to decrease by a factor 2). So we consider that the time interval chosen, even though apparently small when compared to evolution times in heavy ion collisions, is more than enough for the purposes of the paper. Note that such rapid expansion is a

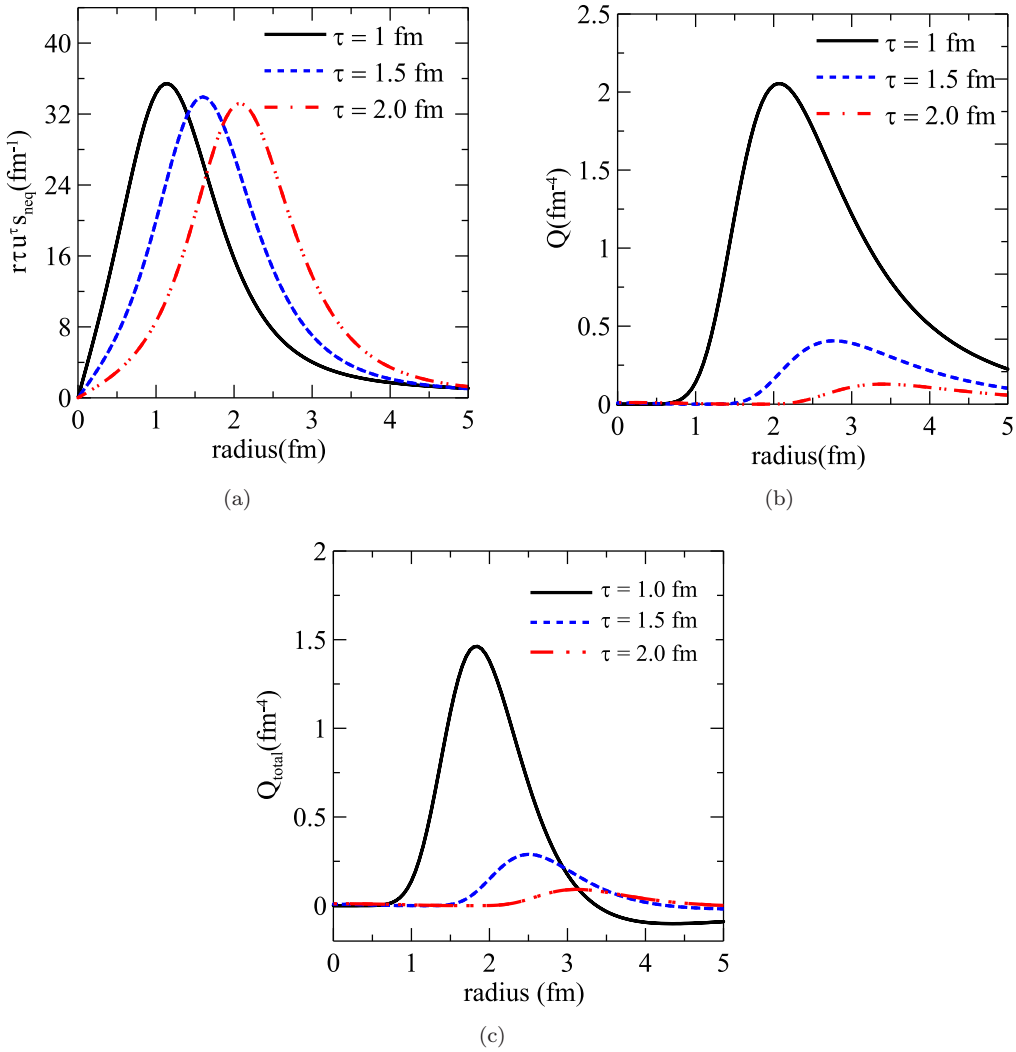

FIG. 3. (Color online) $\tau r u^{\tau} s_{\rm neq}$, entropy production up to second order, Q, and total entropy production, $Q_{\rm total}$, profiles as a function of the radius in Israel-Stewart theory for $\tau = 1$ fm (solid black curves), $\tau = 1.5$ fm (dashed blue curves), and $\tau = 2$ fm (dashed-dotted red curves).

feature of conformal symmetry and may not be present in realistic simulations of heavy ion collisions. For this reason, we do not think that additional time steps are needed. For the comparison with numerical simulations, performed in the next sections, running additional time steps would be numerically (extremely) expensive and the addition of such plots would not change the conclusions of this paper.

IV. TESTING FLUID DYNAMICS

While there are analytical and semi-analytical solutions of relativistic ideal fluid dynamics [7–10], the same is not the case for Israel-Stewart theory. This makes testing numerical algorithms that solve the equations of relativistic fluid dynamics rather problematic. Procedures such as fixing the numerical viscosity, choosing appropriate parameters for flux limiters, etc., which strongly rely on trial and error, become then highly nontrivial. Furthermore, most algorithms used to numerically solve the equations of Israel-Stewart theory were not developed for this purpose: they were developed to solve conservation laws or even Navier-Stokes theory, usually in the nonrelativistic limit. In practice, most simulation codes used in heavy ion collisions have to adapt such algorithms to also solve Israel-Stewart theory. In this sense, the set of parameters that were found optimal to solve certain problems in the nonrelativistic regime, such as the Riemann problem [26], might not be optimal to solve Israel-Stewart theory in the conditions produced in heavy ion collisions.

In this section, we compare numerical solutions of dissipative fluid dynamics obtained via the Kurganov-Tadmor (KT) algorithm [27] using MUSIC [13], with semi-analytical solutions of (conformal) Israel-Stewart theory in the Gubser flow scenario. We show how this can be used to probe not only the quality and accuracy of the dynamical simulation but also to find the optimal value for some of the (numerical) parameters that exist in the algorithm.

In the standard version of MUSIC, the evolution equations that are solved are already those listed in Eqs. (1), (2), and (3). Therefore, the solutions calculated with MUSIC can already be compared with those of Gubser flow obtained in the previous section. For a meaningful comparison, one must initialize the numerical simulation with an initial condition

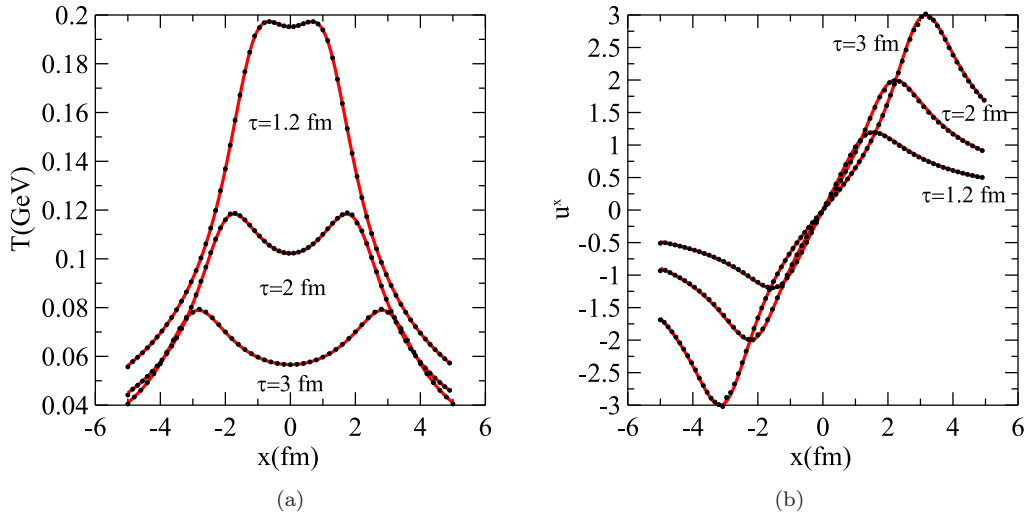

FIG. 4. (Color online) Comparison between the solutions for temperature (left panel) and the x component of the four-velocity (right panel) from Gubser flow and MUSIC (numerical), as a function of x. In this plot $\eta/s = 0.2$ and $\tau_R T = 5\eta/s$. The solid lines denote the semi-analytic solution while the points denote solutions obtained from MUSIC.

constructed from the solutions of Eqs. (11) and (12) for a given initial time. In this work, we fix the initial time to be $\tau_0 = 1$ fm. The temperature at $\rho = 0$, which determines the temperature at $\tau = \tau_0$ and $r = 0$, is fixed to be $T = T_0 = 1.2$ fm^{-1}. The shear-stress tensor at $\rho = 0$ is initialized to be $\pi^{\mu\nu} = 0$. The viscosity in MUSIC is set to $\eta/s = 0.2$ while the relaxation time is fixed to $\tau_R = 5\eta/(\varepsilon + P)$, i.e., $c = 5$. This parametrization for the relaxation time guarantees that the fluid dynamical evolution is causal [19]. The time step and grid spacing used in the numerical simulation are $\delta\tau = 0.005$ fm and $\delta x = \delta y = 0.05$ fm, respectively ($\delta\tau$,δx, and δy are small enough to achieve the continuum limit). We remark that in Gubser flow the values of the transport coefficients actually affect the initial condition of the fluid, since in this scheme the initial condition in hyperbolic coordinates must also be constructed by actually solving the fluid-dynamical equations in the generalized de Sitter space.

Note that MUSIC was originally designed to solve Israel-Stewart theory in 3+1 dimensions, while the Gubser flow solution assumes boost invariance (and radial symmetry in the transverse plane). In a numerical simulation in 3+1 dimensions, boost invariance can be trivially obtained by providing an initial condition that is also boost invariant. In this situation, the solutions of fluid dynamics should maintain exact boost invariance, remaining trivial in the longitudinal direction. We checked that this does occur in the solutions obtained with MUSIC: the temperature and $\pi^{\mu\nu}$ profiles remain (exactly) constant in the ξ direction (e.g., $\pi^{\xi x}$,$\pi^{x\xi}$,$\pi^{\xi y}$,$\pi^{y\xi}$ are exactly zero) while the longitudinal component of the velocity field is exactly zero. This is only not the case at the boundary of the grid where boost invariance is not exactly maintained due to finite size effects.

A. Comparison to semi-analytical solution

In the following we compare the numerical solutions of MUSIC with the semi-analytical solutions of Israel-Stewart theory. Figures 4 and 5 show the spatial profiles of temperature T, velocity u^x, and the $\xi\xi, yy$, and xy components of the shear-stress tensor, $\pi^{\xi\xi}$,π^{yy}, and π^{xy}, respectively. Without loss of generality, T,u^x,$\pi^{\xi\xi}$,π^{yy} are shown as a function of x in the $y = 0$ axis, while the π^{xy} profile is shown as a function of x in the $x = y$ direction. The component π^{xy} vanishes on the x, y axis, which we verified also happens in MUSIC. Note that all the other components of $\pi^{\mu\nu}$ can be obtained from the three components displayed, i.e., $\pi^{\xi\xi}$,π^{yy}, and π^{xy}.

One can see that the agreement between the numerical simulation and the semi-analytical solutions is very good. Only the xy component of the shear-stress tensor displayed some oscillation at late times. However, since this component is small, this oscillation is not enough to spoil the overall agreement.

We remark that such good agreement could only be obtained by adjusting the flux limiter used in the KT algorithm. Flux limiters are employed in MUSCL scheme algorithms, such as the KT algorithm, to control artificial oscillations that usually occur when using higher order discretization schemes for spatial derivatives. Such spurious oscillations are known to appear when resolving shock problems, solutions with discontinuities in density profiles or velocity field, or even when describing systems which display high gradients, such as the system created in relativistic heavy ion collisions. Since dissipative effects originate mainly from spacelike gradients of the velocity field, flux limiters are essential in order to obtain a precise numerical solution of dissipative fluid dynamics.

Currently, there are several flux limiter algorithms available and many others still being developed. In MUSIC, the van Leer minmod filter is used [13]. In this case, the gradients of currents and fluxes are controlled according to a free parameter χ, which may vary from $\chi = 1$ (most dissipative) to $\chi = 2$ (least dissipative). The optimal value of χ can vary case by case and is usually fixed by trial and error; in previous work, MUSIC was run with $\chi = 1.1$. However, the agreement displayed in

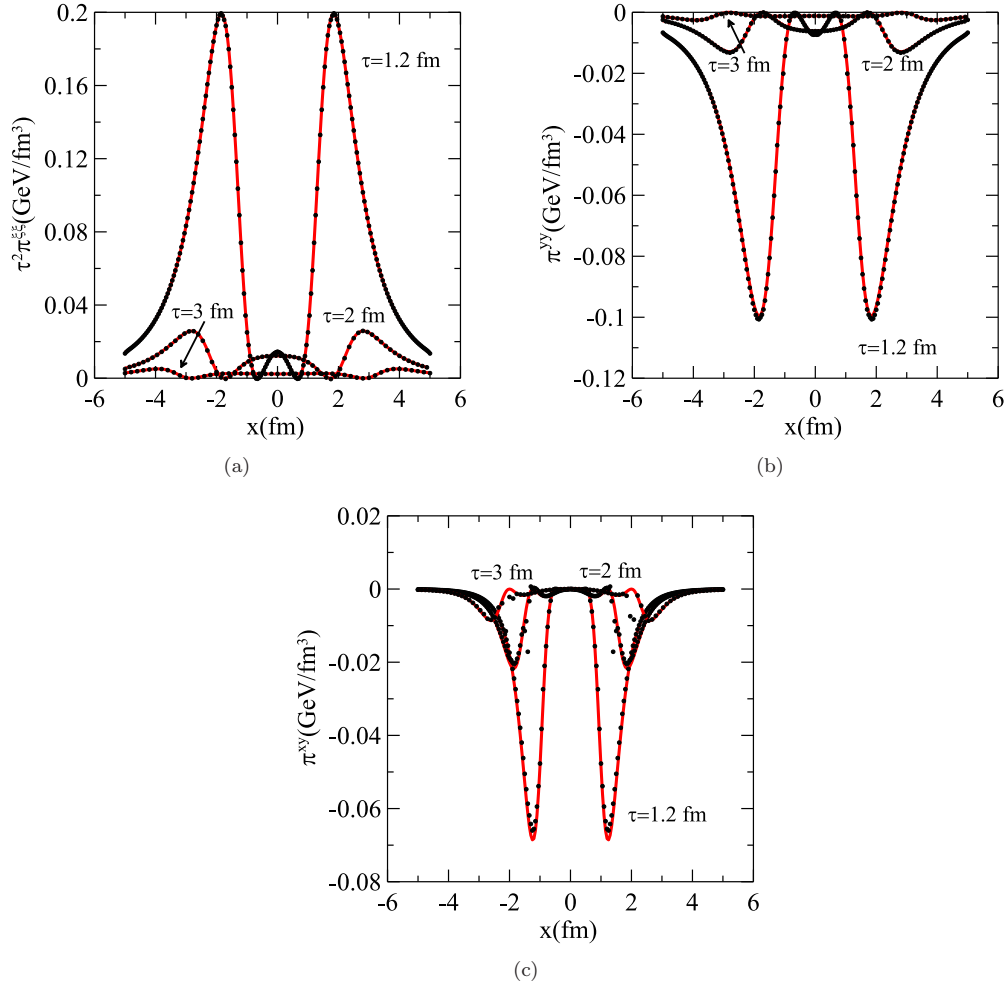

FIG. 5. (Color online) Comparison between the solutions for the $\xi\xi$ (left panel), yy (right panel), and xy (lower panel) components of the shear-stress tensor from Gubser flow and MUSIC (numerical), as a function of x. In this plot $\eta/s = 0.2$ and $\tau_R T = 5\eta/s$. The solid lines denote the semi-analytic solution while the points denote solutions obtained from MUSIC.

Figs. 4 and 5 is only obtained by choosing a larger value, $\chi = 1.8$, corresponding to the less diffusive case. The solutions of the temperature and velocity fields are not very sensitive to changes in the flux limiter scheme. On the other hand, the solutions of the shear-stress tensor do depend on the choice of this numerical parameter. In Fig. 6 we show the numerical solutions of MUSIC obtained with $\chi = 1.1$ (open circles) for the xx and yy components of the shear-stress tensor, which are the components most sensitive to this parameter. These solutions are compared with those of $\chi = 1.8$ (full circles) and the semi-analytical solutions (solid line). One can see that when $\chi = 1.1$ the agreement becomes worse, demonstrating the usefulness of the semi-analytic solution found in this paper in testing the algorithm. It should be noted that, if a flux limiter is not employed at all, it is not possible to properly describe the Gubser flow solutions of Israel-Stewart theory.

Figures 7(a) and 7(b) show the total equilibrium and nonequilibrium entropy (integrated from $r = 0$ to $r = 5$ fm) as a function of time. The entropy is normalized so that its value at $\tau = 1$ fm is equal to 1. The solid (red) line corresponds to the total entropy of the semi-analytical solution, while the circles correspond to the total entropy obtained from our numerical solution. We also included the dashed (blue) and dash-dotted (green) lines in Fig. 7(b), which correspond to the total nonequilibrium entropy integrated over larger volumes, $r = 0$ to $r = 7.5$ fm, and $r = 0$ to $r = 12$ fm, respectively. As one can see, the agreement between the total entropy obtained from the numerical solution and the semi-analytic solution is very good, indicating a negligible amount of numerical entropy production in the simulation. As already mentioned, the equilibrium entropy does not satisfy the second law of thermodynamics, so it does not have to increase with time. On the other hand, the nonequilibrium entropy is expected to increase with time as long as the $\mathcal{O}(4)$ term in Eq. (20) remains small. As shown in the previous section, the overall entropy produced in the range $r = 0 - 5$ fm is positive in the semi-analytical solution, at least for times larger than $\tau = 1$ fm. Note that we do not integrate the nonequilibrium entropy density over an infinite volume so, at some point, the integrated nonequilibrium entropy will start to decrease due to the amount of entropy that is leaving the box. This happens for both numerical and semi-analytical solutions around $\tau = 2$ fm.

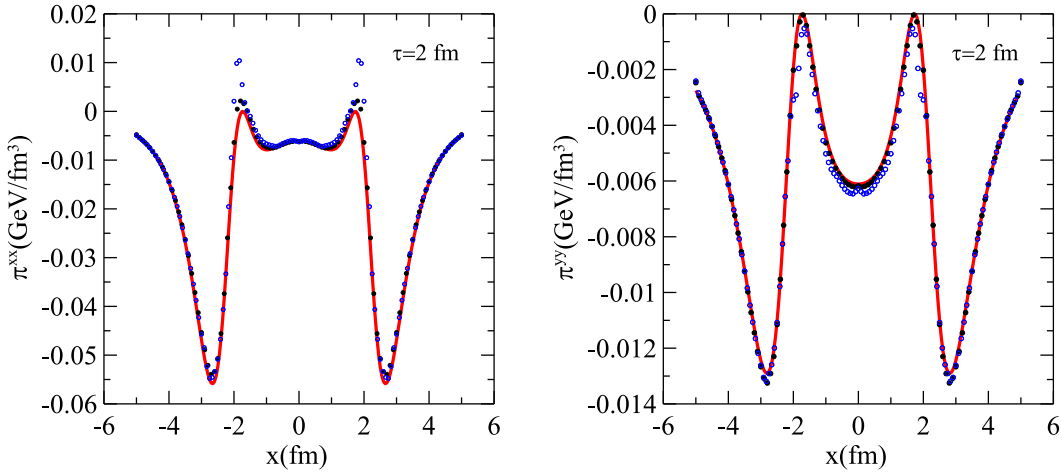

(a) (b)

FIG. 6. (Color online) Numerical solutions of MUSIC obtained with $\chi = 1.1$ (open circles) for the xx (left panel) and yy (right panel) components of the shear-stress tensor. The full circles correspond to the solutions obtained with $\chi = 1.8$ and the solid lines correspond to the semi-analytic solution.

Nevertheless, the agreement between the numerical simulation and the semi-analytical solution remains very good even at these stages.

B. Comparison to analytical solution

In the previous section, we showed that an analytical solution for Israel-Stewart theory can be found in the limit of extremely large viscosity or, equivalently, of extremely small temperatures (cold plasma limit). Note that this analytical solution is no longer an approximation if the term $\pi^{\mu\nu}$ is removed from Israel-Stewart theory; that is, if one solves the equation

$$\frac{\tau_R}{sT}\left(\Delta^{\mu}_{\alpha}\Delta^{\nu}_{\beta}\, D_\tau \pi^{\alpha\beta} + \frac{4}{3}\pi^{\mu\nu}\nabla_\alpha u^\alpha\right) = -\frac{2\eta}{s}\frac{\sigma^{\mu\nu}}{T} \qquad (21)$$

instead of Eq. (3).

The solution of this equation no longer relaxes to Navies-Stokes theory. However, it can still be used to test algorithms that solve relativistic fluid dynamics. The same algorithm that solves Israel-Stewart theory should also be able to solve the above equation of motion and this can be used as an independent and powerful test of a given numerical approach.

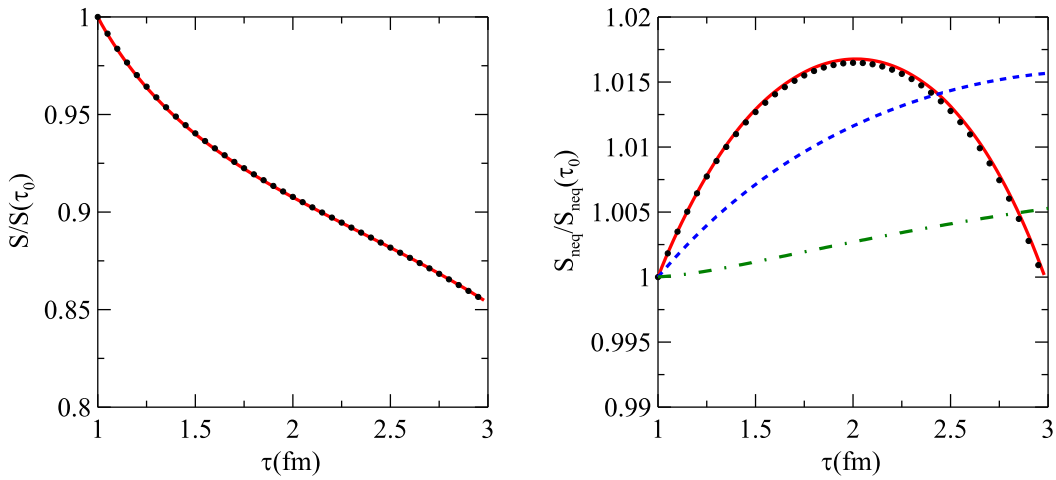

(a) (b)

FIG. 7. (Color online) Comparison between the solutions for the total equilibrium entropy (left panel) and total nonequilibrium entropy (right panel) from Gubser flow and MUSIC (numerical), as a function of τ. In both plots the total entropy is obtained by integrating corresponding entropy density from $r = 0$ to $r = 5$ fm. The solid lines denote the semi-analytic solution while the points denote solutions obtained from MUSIC. On the right panel, we also show the total nonequilibrium entropy obtained by integrating from $r = 0$ to $r = 7.5$ fm (dashed line) and $r = 0$ to $r = 12$ fm (dashed-dotted line).

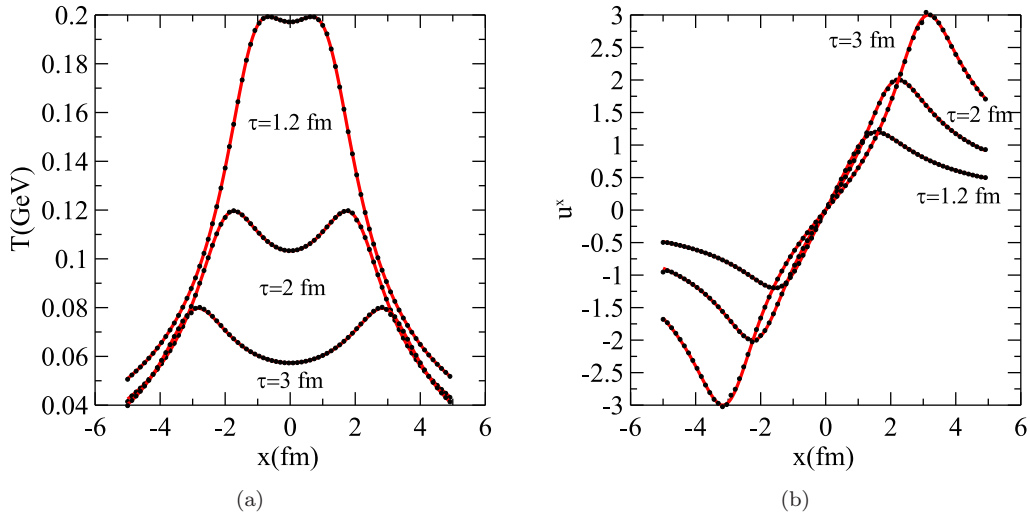

FIG. 8. (Color online) Comparison between the solutions for temperature (left panel) and the x component of the four-velocity (right panel) from Gubser flow and MUSIC (numerical), as a function of x. In this plot $\eta/s = 0.2$ and $\tau_R T = 5\eta/s$. The solid lines denote the analytic solution while the points denote solutions obtained from MUSIC.

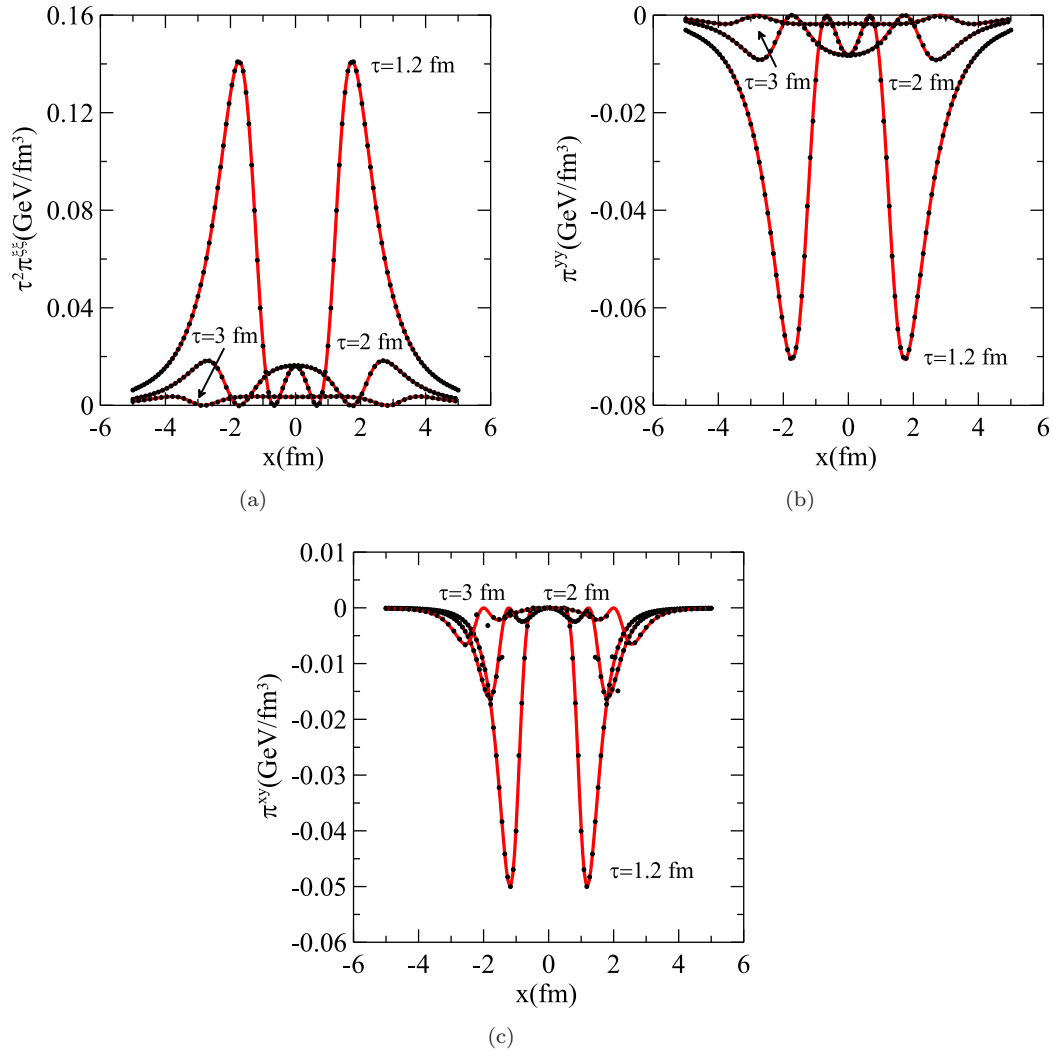

FIG. 9. (Color online) Comparison between the solutions for the $\xi\xi$ (left panel), yy (right panel), and xy (lower panel) components of the shear-stress tensor from Gubser flow and MUSIC (numerical), as a function of x. In this plot $\eta/s = 0.2$ and $\tau_R T = 5\eta/s$. The solid lines denote the analytic solution while the points denote solutions obtained from MUSIC.

Furthermore, the term $\pi^{\mu\nu}$ is rather simple and does not demand much work to be removed.

As already mentioned, in this case the solution of the theory in de Sitter space can be found analytically; see Eqs. (17) and (16). We numerically solved Eqs. (1), (2), and (21) using MUSIC by subtracting the aforementioned term, using the same initial condition described before. The comparison is showed in Figs. 8 and 9, which show the spatial profiles of T,u^x,$\pi^{\xi\xi}$,π^{yy}, and π^{xy}. The solid lines correspond to the analytical solutions while the points correspond to the numerical solutions of Eq. (21) obtained with MUSIC.

Note that the level of agreement is the same as before. The solutions in hyperbolic coordinate even appear to be qualitatively the same, containing the same general structures as the full solutions. However, from a practical point of view, the above solutions are very convenient to test a code since they are already cast in the form of functions and can be written directly into the code.

V. CONCLUSIONS

We have presented the first analytical and semi-analytical solutions of a radially expanding viscous conformal fluid that follows relaxation-type equations such as the Israel-Stewart equations. The $SO(3) \otimes SO(1,1) \otimes Z_2$ invariant solutions for the temperature, shear stress tensor, and flow discussed here can be used to test the existing numerical algorithms used to solve the equations of motion of viscous relativistic fluid dynamics in ultrarelativistic heavy ion collision applications.

We further demonstrated how the solutions derived in this paper can be used to optimize the numerical algorithm of a well known hydrodynamical code, fixing numerical parameters that can only be determined by trial and error. The MUSIC simulation code was shown to produce results that are in good agreement with the analytic and semi-analytic solutions of Israel-Stewart theory undergoing Gubser flow.

Also, once the temperature and shear-stress tensor profiles are known, one can use this information for instance to study the energy loss of hard probes in a radially expanding and viscous QGP scenario [28,29]. Another interesting aspect that could be studied would be the propagation of small disturbances [12,30] on the expanding Israel-Stewart fluid background found here in which the temperature is positive definite throughout the whole dynamical evolution (which is not the case in the Navier-Stokes solution). Moreover, it would be interesting to see if the solutions found here for the conformal Israel-Stewart equations correspond to a black hole configuration in an asymptotically AdS_5 geometry, as it is the case for the Navier-Stokes equations at zero chemical potential [31].

It is important to emphasize that the solutions found in this paper assume boost invariance and, consequently, can only test a limited part of the algorithms employed in $3+1$D fluid-dynamical simulation codes. In order to test the discretization in the longitudinal direction, one would require analytical or semi-analytical solutions of Israel-Stewart theory that are not boost invariant. Recently, the first full $3+1$D analytical solutions of second-order conformal hydrodynamics have been obtained in [32,33] and one may use them in the future to check the accuracy of $3+1$D viscous hydrodynamic codes.

ACKNOWLEDGMENTS

The authors acknowledge many useful exchanges with B. Schenke, and are grateful to I. Kozlov, J.-F. Paquet, D. H. Rischke, J.-B. Rose, and G. Vujanovic for discussions. This work was funded in part by Fundaçã o de Amparo à Pesquisa do Estado de São Paulo (FAPESP), in part by Conselho Nacional de Desenvolvimento Científico e Tecnológico (CNPq), and in part by the Natural Sciences and Engineering Research Council of Canada. G.S.D. acknowledges the support of a Banting fellowship provided by the Natural Sciences and Engineering Research Council of Canada.

[1] M. Gyulassy and L. McLerran, Nucl. Phys. A **750**, 30 (2005).
[2] U. W. Heinz and R. Snellings, Annu. Rev. Nucl. Part. Sci. **63**, 123 (2013).
[3] C. Gale, S. Jeon, and B. Schenke, Int. J. Mod. Phys. A **28**, 1340011 (2013).
[4] W. A. Hiscock and L. Lindblom, Ann. Phys. (NY) **151**, 466 (1983); Phys. Rev. D **31**, 725 (1985); **35**, 3723 (1987); Phys. Lett. A **131**, 509 (1988).
[5] W. Israel, Ann. Phys. (NY) **100**, 310 (1976); W. Israel and J. M. Stewart, *ibid.* **118**, 341 (1979).
[6] L. D. Landau and E. M. Lifshitz, *Fluid Mechanics*, 2nd ed., Course of Theoretical Physics Vol. 6 (Butterworth-Heinemann, Oxford, 1987).
[7] J. D. Bjorken, Phys. Rev. D **27**, 140 (1983).
[8] T. Csorgo, F. Grassi, Y. Hama, and T. Kodama, Phys. Lett. B **565**, 107 (2003).
[9] T. Csorgo, L. P. Csernai, Y. Hama, and T. Kodama, Heavy Ion Phys. A **21**, 73 (2004).
[10] T. Csorgo, M. I. Nagy, and M. Csanad, Phys. Lett. B **663**, 306 (2008).
[11] S. S. Gubser, Phys. Rev. D **82**, 085027 (2010).
[12] S. S. Gubser and A. Yarom, Nucl. Phys. B **846**, 469 (2011).
[13] B. Schenke, S. Jeon, and C. Gale, Phys. Rev. C **82**, 014903 (2010); Phys. Rev. Lett. **106**, 042301 (2011); Phys. Rev. C **85**, 024901 (2012).
[14] R. Baier, P. Romatschke, D. T. Son, A. O. Starinets, and M. A. Stephanov, J. High Energy Phys. 04 (2008) 100.
[15] J. Noronha and G. S. Denicol, arXiv:1104.2415.
[16] G. Aad *et al.* (ATLAS Collaboration), Phys. Rev. C **86**, 014907 (2012).
[17] S. Chatrchyan *et al.* (CMS Collaboration), J. High Energy Phys. 02 (2014) 088.
[18] G. S. Denicol, T. Kodama, T. Koide, and P. Mota, J. Phys. G **35**, 115102 (2008).
[19] S. Pu, T. Koide, and D. H. Rischke, Phys. Rev. D **81**, 114039 (2010).

[20] M. Luzum and J.-Y. Ollitrault, Nucl. Phys. A **904–905**, 377c (2013).
[21] G. S. Denicol, T. Koide, and D. H. Rischke, Phys. Rev. Lett. **105**, 162501 (2010).
[22] G. S. Denicol, J. Noronha, H. Niemi, and D. H. Rischke, Phys. Rev. D **83**, 074019 (2011).
[23] G. S. Denicol, H. Niemi, E. Molnar, and D. H. Rischke, Phys. Rev. D **85**, 114047 (2012).
[24] P. K. Kovtun, D. T. Son, and A. O. Starinets, Phys. Rev. Lett. **94**, 111601 (2005).
[25] P. Romatschke, Class. Quantum Grav. **27**, 025006 (2010).
[26] D. H. Rischke, Y. Pursun, and J. A. Maruhn, Nucl. Phys. A **595**, 383 (1995); **596**, 717(E) (1996); D. H. Rischke, Lect. Notes Phys. **516**, 21 (1999); E. Molnar, H. Niemi, and D. H. Rischke, Eur. Phys. J. C **65**, 615 (2010); Y. Akamatsu, S.-i. Inutsuka, C. Nonaka, and M. Takamoto, J. Comput. Phys. **256**, 34 (2014); I. Bouras, E. Molnar, H. Niemi, Z. Xu, A. El, O. Fochler, C. Greiner, and D. H. Rischke, Phys. Rev. C **82**, 024910 (2010); L. Del Zanna *et al.*, Eur. Phys. J. C **73**, 2524 (2013).
[27] A. Kurganov and E. Tadmor, J. Comput. Phys. **160**, 241 (2000); R. Naidoo and S. Baboolal, Future Generat. Comput. Syst. **20**, 465 (2004).
[28] B. Betz and M. Gyulassy, arXiv:1305.6458.
[29] B. Schenke, C. Gale, and S. Jeon, Phys. Rev. C **80**, 054913 (2009).
[30] P. Staig and E. Shuryak, Phys. Rev. C **84**, 044912 (2011).
[31] S. Bhattacharyya, S. Minwalla, V. E. Hubeny, and M. Rangamani, J. High Energy Phys. 02 (2008) 045.
[32] Y. Hatta, J. Noronha, and B.-W. Xiao, Phys. Rev. D **89**, 051702 (2014).
[33] Y. Hatta, J. Noronha, and B.-W. Xiao, Phys. Rev. D **89**, 114011 (2014).